NANO LETTERS

pubs.acs.org/NanoLett

# Energy Transfer from an Individual Quantum Dot to a Carbon Nanotube

**Eyal Shafran, Benjamin D. Mangum,† and Jordan M. Gerton***

Department of Physics and Astronomy, University of Utah, Salt Lake City, Utah 84112

**ABSTRACT** Precision measurements of resonant energy transfer from isolated quantum dots (QDs) to individual carbon nanotubes (CNTs) exhibit unique features due to the one-dimensional nature of CNTs. In particular, excitons can be created at varying distances from the QD at different locations along the CNT length. This leads to large variations in energy transfer length scales for different QDs and a novel saturation of the energy transfer efficiency at ~96%, seemingly independent of CNT chirality.

**KEYWORDS** Nano-optics, energy transfer, FRET, nanotube, quantum dot, fluorescence quenching

A detailed understanding of energy transduction is crucial for achieving precise control of energy flow in complex, integrated systems. In this context, carbon nanotubes (CNTs) are intriguing model systems due to their rich, chirality-dependent electronic and optical properties.[1−3] Recently, hybrid materials composed of quantum dots (QDs) attached to CNTs have been synthesized for a wide range of applications,[4−9] including photovoltaics, nanotherapeutics, bioimaging, and photocatalysis. Each component has unique properties that make their combination highly desirable: QDs have broad absorption spectra and size-tunable emission spectra,[10] while CNTs can be metallic with ballistic 1D charge transport, or semiconducting depending on the chiral angle of the underlying graphene lattice.[1,3] The interfacial area in these materials should be extremely large due to the large surface to volume ratio of both QDs and CNTs, so interactions between them are very important for their overall behavior. In particular, the fluorescence emission from QDs is strongly suppressed when they are attached to CNTs, which indicates strong coupling between them. Heretofore, it has not been possible to unambiguously attribute the reduced fluorescence to either charge or energy transfer between the QDs and CNTs or to establish limits on the coupling efficiency. If QD−CNT composites are indeed to be pursued for various optoelectronic applications, it is clearly important to understand the energy transduction pathways in more detail.

It is difficult to extract a detailed understanding of the underlying energy transduction mechanisms using ensembles of QDs attached to CNTs. Therefore, we adopt a single-particle approach whereby we measure the interaction between single QD-CNT pairs. CNTs are first attached to atomic force microscope (AFM) probes via the "pickup" technique,[11] and are then brought into close proximity to isolated QDs illuminated with a laser beam of well-defined polarization (Figure 1a). In a typical experiment, the CNT tip is aligned into the center of the focal spot and the sample is raster-scanned until a QD is located topographically with atomic force microscopy (AFM). An optical image is then acquired using a unique photon counting technique[12,13] whereby each detected photon is correlated with the instantaneous vertical and lateral position of the CNT tip relative to the surface of the QD as the tip oscillates vertically in intermittent contact mode with a typical peak−peak amplitude of 40−100 nm. A histogram of photon count rates as a function of tip height, normalized to the rate measured at the far-point of the tip oscillation, is accumulated at each lateral position, producing a 3D data set. The 2D ($x$−$z$) fluorescence image in Figure 1b demonstrates that CNTs attached to AFM probes can be used for nanometer-scale energy transfer microscopy;[14] QD-functionalized probes have been used in a similar manner previously.[15] 1D approach curves can also be extracted from the same 3D data set[13] or by halting the lateral scan when the CNT is centered above the QD (Figure 2c).

For this work, six CNTs with final protrusion lengths ranging from $L = 50$ nm to $L = 165$ nm were used for ~110 high-precision measurements of CdSe/ZnS QD fluorescence as a function of the CNT−QD separation. The chemical vapor deposition growth recipe used to produce our CNT pickup substrates has been shown to produce almost exclusively single-walled CNTs.[16] On the basis of the expected distribution of CNT chiralities on the growth substrates, there should be both metallic and semiconducting varieties within our sample of picked up nanotubes.[1,17] CNTs that are not oriented within ~10 degrees of the vertical axis (i.e., along $z$ in Figure 1a) tend to buckle under compression during intermittent contact[18] and are not useful for AFM imaging. Thus, it is safe to approximate the CNTs used in these experiments as being vertically oriented.

* To whom correspondence should be addressed, jgerton@physics.utah.edu.

† Current address: Soft Matter Nanotechnology and Advanced Spectroscopy Team, Los Alamos National Laboratory, Los Alamos, NM 87545.

**Received for review: 06/9/2010**
**Published on Web: 00/00/0000**





DOI: 10.1021/nl102045g | *Nano Lett.* **XXXX,** *xxx,* 000–000

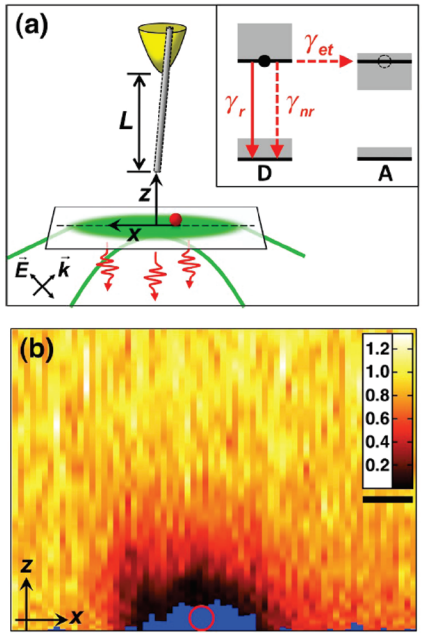


FIGURE 1. Experimental scheme. (a) A CNT protrudes a distance $L$ beyond a gold-coated probe. The probe oscillates along $z$ as an isolated QD is scanned along $x$. The sample is illuminated with an evanescent field via a focused laser beam whose wave-vector k is beyond the critical angle for total internal reflection. The polarization of the evanescent wave can be parallel (as shown) or perpendicular to the CNT axis depending on the incident field direction E. A high numerical-aperture lens (not shown) focuses the laser beam and collects the QD emission through a glass coverslip. The inset shows a generic level scheme for energy transfer between a donor (D) and acceptor (A): The energy transfer rate $\gamma_{et}$ competes with the intrinsic relaxation of the QD, $\gamma_0 = \gamma_r + \gamma_{nr}$. (b) Combined topographical and fluorescence image in an $x-z$ plane containing the QD. The CNT traces out the topographical signal indicated by the blue cutout; the red circle denotes the physical size of the QD. The fluorescence signal is normalized to that at the point of maximum CNT−QD separation, as given by the color scale. The scale bar corresponds to 10 nm.

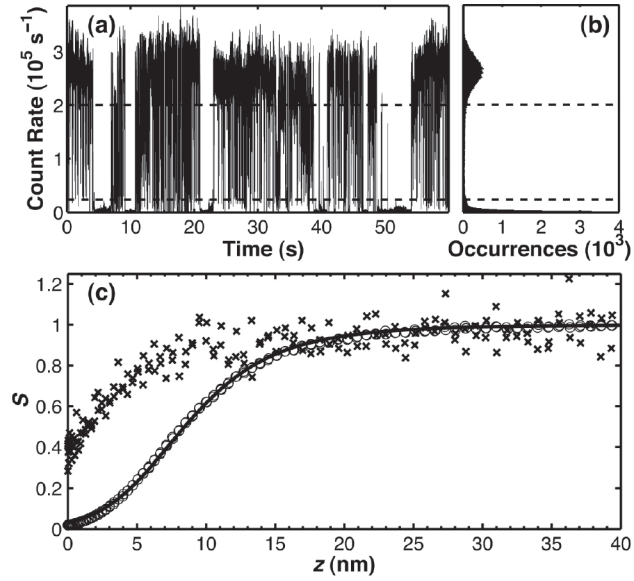


FIGURE 2. Typical approach curves for bright and dark states of a QD. (a) 60 s fluorescence trajectory of a QD demonstrating intermittent changes in its quantum yield. (b) Histogram of count rates using 1 ms time bins. The upper and lower horizontal dashed lines delineate thresholds for the bright and dark states, respectively. (c) Vertical approach curves corresponding to the bright (open circles) and dark (cross) states. The solid line corresponds to a fit to eq 3 with $R_0 = 19.1$ nm and $z_0 = 10.6$ nm.

All six of the CNTs used for this work induce strong quenching of the QD fluorescence at small CNT−QD separations (<25 nm), an example of which is shown in Figure 1b. In addition, lower precision measurements obtained over the last several years using more than 50 CNTs uniformly exhibit similarly strong quenching (data not shown). Only two mechanisms can lead to the observed quenching: energy transfer and charge transfer. Energy transfer can occur when an exciton in the QD resonantly excites an excitation in the CNT via electromagnetic coupling, as in Förster (fluorescence) resonance energy transfer (FRET). In this case, there is no net exchange of charge, resulting in a neutral excitation such as an exciton or plasmon within the CNT. In charge transfer, an electron is exchanged and the resulting excitation within the CNT is associated with an electric current. There are two main signatures in the QD fluorescence signal that can be used to discriminate between these two mechanisms. First, a charged QD will exhibit a relatively low quantum yield (dark state) until it is neutralized, since excitons within a charged QD undergo fast nonradiative relaxation via an Auger recombination process.[19] Our experiments are performed on glass substrates, so the neutralization time is likely to be a large fraction of the tip oscillation period (~10 $\mu$s), and charging of the QD via electron transfer should produce a delay in the recovery of fluorescence following intermittent contact of the CNT and QD. Only very rarely is this effect observed[14] and never for the data presented here. Second, fluorescence blinking in QDs is thought to be caused by charging of the core via the intermittent trapping of an exciton's electron or hole at the interface. Therefore, the fluorescence blinking dynamics for a charged QD should be altered substantially. An analysis of the blinking statistics of QDs in the presence and absence of CNTs reveals no significant difference in these two cases (supplementary Figure S1 in Supporting Information). Thus, we conclude that the dominant quenching mechanism for these experiments is resonant energy transfer, in agreement with several previous studies of fluorescence quenching near nanostructures.[20−23]

Since energy transfer competes with the intrinsic radiative and nonradiative relaxation processes in the QD (Figure 1a inset), the normalized fluorescence signal ($S$) is generically described by

$$S = \frac{Q(r)}{Q_0} = \frac{\gamma_0}{\gamma_0 + \gamma_{et}(r)} = \frac{1}{1 + \gamma_{et}/\gamma_0} \qquad (1)$$



DOI: 10.1021/nl102045g | Nano Lett. XXXX, xxx, 000−000

where $Q(r) = \gamma_r/[\gamma_0 + \gamma_{et}(r)]$ is the quantum yield of the QD, which depends on the position, $r$, of the CNT terminus relative to the QD surface, $\gamma_r$ is the intrinsic radiative relaxation rate of the QD, $\gamma_0 = \gamma_r + \gamma_{nr}$ is the far-field fluorescence rate, $\gamma_{nr}$ is the intrinsic nonradiative relaxation rate, $\gamma_{et}(r)$ is the position-dependent energy transfer rate, and $Q_0 = \gamma_r/\gamma_0$ is the far-field quantum yield. The optical excitations within CNTs have been shown to be excitonic in nature,[24−27] even for metallic CNTs due to reduced electron screening.[28,29] Thus, the normalized energy transfer rate is given by the Förster theory for dipole−dipole coupling[30]

$$\frac{\gamma_{et}}{\gamma_0} = Q_0\frac{\gamma_{et}}{\gamma_r} = \left(\frac{R_0}{r}\right)^6 \tag{2}$$

where $R_0$ is the Förster radius and $r$ is the distance between two point dipoles, the donor and acceptor.

Previous work has suggested that the coupling between a dipole emitter and a nanotube or nanowire should result in a lower-order dependence of the energy transfer rate on distance, (e.g., $r^{-5}$).[23] This results from an integration of the coupling strength along the nanotube and is appropriate if excitations can be created anywhere along the length of the CNT with equal probability. Indeed, previous theoretical treatments only considered a geometry where the emitter was located near a (semi)infinite, defect-free CNT at a particular radial distance from its axis, in which case the assumption of uniformity is valid.[20,22,23] In our case, the emitter (QD) is located along the CNT axis very close to and beneath its terminus. This edge discontinuity disrupts the uniform excitation distribution, which invalidates a $r^{-5}$ energy transfer dependence for our geometry. In the absence of an explicit model applicable to our unique situation, and with the knowledge that the dominant excitations within CNTs at optical frequencies are strongly localized excitons, we adopt a simple model whereby the energy transfer is a stochastic process that occurs between point dipoles with a probability derived from eq 2. As described in detail below, this model agrees remarkably well with measurements and allows for novel interpretation of the data.

$R_0$ depends on a number of factors, including the integrated overlap of donor-emission and acceptor-absorption spectra and the relative orientation of the donor and acceptor transition dipole moments. The explicit dependence on $Q_0$ given in eq 2 implies that even for a specific CNT, the position dependence of $S$ will vary from one QD to another and also for a particular QD during fluorescence blinking and/or oxidation-induced decay. It is important to recognize that for every photoexcitation cycle, the QD will relax either via intrinsic processes *or* via energy transfer to the CNT. Thus, the rates for intrinsic relaxation ($\gamma_0$) and energy transfer ($\gamma_{et}$) in eq 2 are averaged over many photoexcitation/energy transfer cycles. Furthermore, each time an energy transfer event occurs, one quantum of energy will be transferred to the CNT in the form of an exciton, which can be created anywhere along the length of the CNT. Therefore, even when the CNT and QD are in contact, the average separation between donor and acceptor dipoles will generally be nonzero due to the physical size of the QD and the average distance above the CNT terminus at which an exciton is generated. For a vertically aligned CNT centered above a QD, the normalized signal should then be

$$S = \left[1 + \left(\frac{R_0}{z + z_0}\right)^6\right]^{-1} \tag{3}$$

where $z$ is the vertical distance of the CNT terminus from the QD surface and $z_0$ is the effective separation between the donor and acceptor dipoles at $z = 0$.

As the photon histograms are collected, a QD will undergo a series of rapid transitions from a strongly emissive (bright) state to a weakly emissive (dark) one.[31,19] To simplify interpretation of the data, the photon signal is divided into temporal sections corresponding to bright and dark states using a simple threshold procedure, and separate approach curves are accumulated for each (Figure 2). The dark-state signal shows weaker fluorescence suppression since energy transfer competes less effectively with rapid internal nonradiative decay. To avoid convoluting the analysis, only the bright-state data are compared with the modified Förster model.

The solid curve shown in Figure 2c is the best fit to eq 3 for a particular measurement. The high quality of the fit is typical, and Figure 3a shows a summary of $R_0$ and $z_0$ values extracted from model fits for all six CNTs, where each ($z_0$, $R_0$) pair is color coded according to the CNT length, $L$. The fitted values for $R_0$ range from 12 to ∼40 nm, which are much larger than those for molecular fluorophores in FRET experiments. This indicates strong coupling between the QD and CNT, which requires strong absorption by the CNT at $\lambda$ ∼600 nm[2], the emission wavelength for our QDs.

The measured correlation between $z_0$ and $R_0$ evident in Figure 3a is a direct result of the 1D nature of CNTs. In particular, the measured signal at each value of $z$ corresponds to many photoexcitation/energy transfer cycles (see Supporting Information), each of which can result in the creation of an exciton at a different position along the length of the CNT. Stronger coupling between the QD and CNT results in a larger value of $R_0$, which increases the probability for generating an exciton further up the tube. The values of $z_0$ extracted from the model fits are clearly much larger than the sum of the QD radius (∼2 nm) and the exciton radius in the CNT (expected to be 1−4 nm depending on the CNT diameter). Thus, although the exciton is most likely to be created near the CNT terminus where the energy transfer efficiency from the QD is largest, on average it can be created much further up the tube depending on $R_0$.



DOI: 10.1021/nl102045g | *Nano Lett.* **XXXX,** *xxx,* 000−000

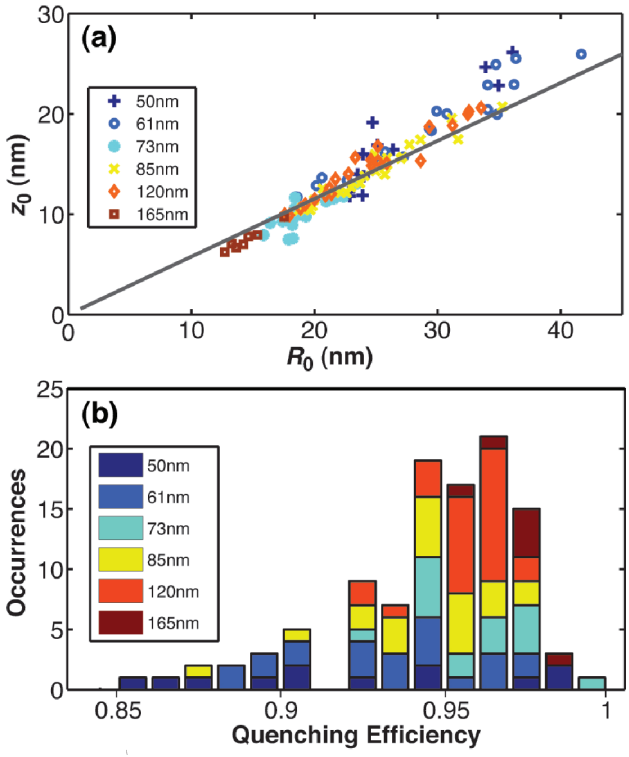


**FIGURE 3. Summary of energy transfer measurements for six CNTs of different lengths. (a) Each point gives the value of $R_0$ and $z_0$ for a particular measurement extracted from a fit to the Förster model. The points are color-coded according to CNT length. The solid line corresponds to $R_0/\sqrt{3}$ as described in the text. (b) Histogram of the measured quenching efficiencies at QD-CNT contact ($z = 0$). These data comprise 110 measurements on 50 different QDs. Most QDs were measured once or twice; a few were measured over five times with a maximum of 14 times (Figure 4).**

A simple estimate of the average position along the CNT at which the exciton is produced can be obtained by calculating the expectation value

$$\langle \zeta \rangle = \frac{\int_z^\infty \zeta E(\zeta, R_0)\, d\zeta}{\int_z^\infty E(\zeta, R_0)\, d\zeta} \qquad (4)$$

where $E(\zeta, R_0) = [1 + (\zeta/R_0)^6]^{-1}$ is the Förster energy transfer efficiency between point dipoles separated by a distance $\zeta$ and $z$ and $R_0$ are as defined above. In this context, $E$ is the probability for an energy transfer event between a donor dipole (an exciton within the QD) and an acceptor dipole (an exciton within the CNT) per photon absorbed by the QD. Evaluating eq 4 at $z = 0$ gives $z_0 \sim \langle \zeta \rangle_{z=0} = R_0/3^{1/2}$, which is plotted as the solid line in Figure 3a. The strong agreement between this simple calculation and the measurements lends confidence to our interpretation of the data.

Interestingly, despite the strength of the QD−CNT coupling, the correlation between $R_0$ and $z_0$ causes the energy transfer efficiency to saturate at $z = 0$, in contrast to the

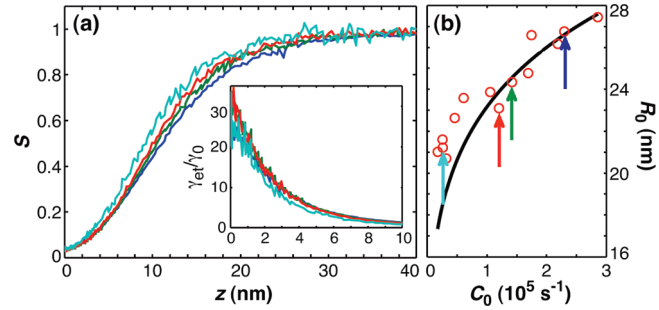


**FIGURE 4. Energy transfer measurements during QD aging. (a) Sample of four approach curves showing a continual decrease in $R_0$ as $Q_0$ degrades. The inset shows $\gamma_{et}/\gamma_0 = 1/S - 1$ for the corresponding approach curves, where the horizontal axis units are nanometers. (b) Fitted values of $R_0$ as a function of the far-field photon count rate, $C_0$, where the data points highlighted by arrows correspond to the approach curves in (a). As the QD ages over a period of ~20 min, $C_0$ decreases monotonically by a factor of ~10, so the data were acquired in order from right to left. Each of the 14 data points in (b) and each separate curve in (a) correspond to a measurement of ~1 min in duration. Between each measurement, the CNT is recentered onto the QD, which takes up to 30 s. Thus it takes ~20 min to complete the 14 measurements.**

FRET efficiency between two point dipoles, which diverges at zero separation. In fact, the simple analysis above predicts that the energy transfer efficiency, $1 - S_{z=0}$, should saturate at a value of $(1 + 3^{-3})^{-1} \cong 0.96$, independent of $R_0$. Figure 3b shows a stacked histogram for the *measured* values of the energy transfer efficiency at $z = 0$ for each CNT. There is no obvious dependence of these measurements on CNT length and, importantly, the peak energy transfer efficiency for every CNT is consistent with the predicted value of 0.96. Despite the large dynamic range in $R_0$, which reflects variations in QD−CNT coupling strength, the peak energy transfer efficiency is tightly constrained. An important consequence of this self-limiting behavior is that the peak energy transfer efficiency should be largely independent of CNT chirality, QD−CNT spectral overlap, and the precise alignment of the QD and CNT transition dipole moments. Since it is still very difficult to selectively grow or separate CNTs based on their chiralities, this point may be crucial in terms of using QD−CNT composites for light-harvesting applications.

It is important to recognize that each CNT in Figure 3 was used to measure several individual QDs, each of which likely had a different intrinsic quantum yield, $Q_0$. Such differences should cause $R_0$ to vary in proportion to $Q_0^{1/6}$ (eq 2), while $R_0$ is not sensitive to disparities in the absorption cross section from one QD to another since the fluorescence data are normalized in a self-consistent manner. In addition to variations between QDs, oxidative damage can decrease $Q_0$ for a particular QD as it ages under ambient conditions.[32] Figure 4a shows a sample of four approach curves for a particular QD as it ages over a period of ~20 min during which a constant illumination intensity was maintained. Also shown in Figure 4b are the values of $R_0$ extracted from all the measurements during this time as a function of the far-field photon count rate, $C_0$, and a solid line that is propor-



DOI: 10.1021/nl102045g | *Nano Lett.* **XXXX,** *xxx,* 000–000

tional to $C_0^{1/6}$. A reduction in the absorption cross section[33] for long aging times (i.e., small values of $C_0$) would tend to push the data to the left of this line, in agreement with the measurements.

Despite the strong correlation between $R_0$ and $C_0$, the energy transfer efficiency saturates at ~0.96; indeed these data are a subset of those plotted in Figure 3. The inset in Figure 4a plots the ratio $\gamma_{et}/\gamma_0 = 1/S - 1$, which is very sensitive to minute variations when $S$ becomes small (i.e., near $z = 0$). The remarkable consistency of the saturation value leads to the important conclusion that as $\gamma_0$ increases during aging (due to an increase in $\gamma_{nr}$), the peak energy transfer rate $\gamma_{et}(z = 0)$ increases proportionally. In FRET experiments between two point dipoles, a smaller value of $R_0$ indicates weaker coupling between the donor and acceptor, generally implying a smaller energy transfer rate. Here, however, the one-dimensional nature of the CNT leads to a different interpretation: *smaller* values of $R_0$ yield *higher* average energy transfer rates upon repeated excitation cycles. This occurs because when $R_0$ is small, the effective center of mass of the exciton distribution within the CNT, $\langle\zeta\rangle$, is *closer* to the end of the CNT and thus closer to the QD, which elevates the *average* energy transfer rate. Within this context, the maximum possible energy transfer rate should occur in the limit that all acceptor excitons are created as close to the QD as possible, i.e., at the tip of the CNT. This corresponds to a minimum dipole−dipole separation $z_{min} \geq 3$ nm: 2 nm for the radius of the QD and ≥1 nm for the exciton radius in the CNT. When $R_0$ becomes smaller than about $\sqrt{3}z_{min}$, then the exciton center of mass cannot adjust toward the CNT tip any further. Beyond this point, the energy transfer rate cannot become any larger and the energy transfer efficiency will decrease. Evidently, the slow degradation in $Q_0$ for the QD in Figure 4 is not sufficient to achieve these conditions and the energy transfer efficiency maintains a saturation value of 0.96. Dark states that occur during blinking can have sufficiently small values of $Q_0$, however, leading to reduced energy transfer efficiency (e.g., Figure 2c).

In conclusion, we have made high-precision measurements of energy transfer from QDs to CNTs and have developed a simple model based on dipole−dipole coupling between excitons to explain the observed behavior. Due to the one-dimensional nature of the CNT, the data exhibit novel features that depart from classical Förster theory for energy transfer between point dipoles. In particular, we observe a strong correlation between the measured length scale ($R_0$) for efficient energy transfer and the average position of the exciton generated within the CNT ($z_0$). This leads to a narrow distribution of the peak energy transfer efficiency and a counterintuitive increase in the energy transfer rate for smaller values of $R_0$. Finally, both the model and measurements suggest that the peak energy transfer efficiency should be independent of CNT chirality, which has important implications with regard to the development of QD−CNT composite materials for light-harvesting applications.

**Acknowledgment.** The authors gratefully acknowledge helpful discussions with Eugene Mishchenko, Mikhail Raikh, and Dane McCamey and thank Yoshie Narui of Caltech for providing a CNT pickup wafer. This work was supported by a Cottrell Scholar Award from the Research Corporation for Science Advancement and NSF CAREER Award Number DBI-0845193.

**Supporting Information Available.** Description of methods used and discussion of evidence against charge transfer, possible systematic effects, normalization procedure, dependence on illumination polarization, and nanotube buckling. This material is available free of charge via the Internet at http://pubs.acs.org.

## REFERENCES AND NOTES

(1) Saito, R.; Dresselhaus, G.; Dresselhaus, M. S. *Physical Properties of Carbon Nanotubes*; Imperial College Press: London, 1998.
(2) Bachilo, S.; Strano, M.; Kittrell, C.; Hauge, R.; Smalley, R.; Weisman, R. *Science* **2002**, *298*, 2361–2366.
(3) Avouris, P.; Freitag, M.; Perebeinos, V. *Nat. Photonics* **2008**, *2*, 341–350.
(4) Biju, V.; Itoh, T.; Baba, Y.; Ishikawa, M. *J. Phys. Chem. B* **2006**, *110*, 26068–26074.
(5) Grzelczak, M.; Correa-Duarte, M.; Salgueirino-Maceira, V.; Giersig, M.; Diaz, R.; Liz-Marzan, L. *Adv. Mater.* **2006**, *18*, 415.
(6) Haremza, J.; Hahn, M.; Krauss, T. *Nano Lett.* **2002**, *2*, 1253–1258.
(7) Olek, M.; Busgen, T.; Hilgendorff, M.; Giersig, M. *J. Phys. Chem. B* **2006**, *110*, 12901–12904.
(8) Li, F.; Son, D. I.; Kim, T. W.; Ryu, E.; Kim, S. W.; Lee, S. K.; Cho, Y. H. *Appl. Phys. Lett.* **2009**, *95*, 061911.
(9) Peng, X.; Chen, J.; Misewich, J. A.; Wong, S. S. *Chem. Soc. Rev.* **2009**, *38*, 1076–1098.
(10) Norris, D. J.; Bawendi, M. G. *Phys. Rev. B* **1996**, *53*, 16338.
(11) Hafner, J.; Cheung, C.; Oosterkamp, T.; Lieber, C. *J. Phys. Chem. B* **2001**, *105*, 743–746.
(12) Gerton, J. M.; Wade, L. A.; Lessard, G. A.; Ma, Z.; Quake, S. R. *Phys. Rev. Lett.* **2004**, *93*, 180801.
(13) Mangum, B. D.; Shafran, E.; Mu, C.; Gerton, J. M. *Nano Lett.* **2009**, *9*, 3440–3446.
(14) Mu, C.; Mangum, B. D.; Xie, C.; Gerton, J. M. *IEEE J. Sel. Top. Quantum Electron.* **2008**, *14*, 206–216.
(15) Ebenstein, Y.; Mokari, T.; Banin, U. *J. Phys. Chem. B* **2004**, *108*, 93–99.
(16) Wade, L.; Shapiro, I.; Ma, Z.; Quake, S.; Collier, C. *Nano Lett.* **2004**, *4*, 725–731.
(17) Narui, Y.; Ceres, D. M.; Chen, J.; Giapis, K. P.; Collier, C. P. *J. Phys. Chem. C* **2009**, *113*, 6815–6820.
(18) Solares, S.; Matsuda, Y.; Goddard, W. *J. Phys. Chem. B* **2005**, *109*, 16658–16664.
(19) Gómez, D. E.; Califano, M.; Mulvaney, P. *Phys. Chem. Chem. Phys.* **2006**, *8*, 4989–5011.
(20) Bondarev, I. V.; Slepyan, G. Y.; Maksimenko, S. A. *Phys. Rev. Lett.* **2002**, *89*, 115504.
(21) Yoskovitz, E.; Oron, D.; Shweky, I.; Banin, U. *J. Phys. Chem. C* **2008**, *112*, 16306.
(22) Hernández-Martínez, P.; Govorov, A. *Phys. Rev. B* **2008**, *78*, 035314.
(23) Swathi, R. S.; Sebastian, K. L. *J. Chem. Phys.* **2010**, *132*, 104502.
(24) Korovyanko, O.; Sheng, C.; Vardeny, Z.; Dalton, A.; Baughman, R. *Phys. Rev. Lett.* **2004**, *92*, 017403.
(25) Wang, F.; Dukovic, G.; Brus, L.; Heinz, T. *Science* **2005**, *308*, 838–841.
(26) Ando, T. *J. Phys. Soc. Jpn.* **1997**, *66*, 1066–1073.



DOI: 10.1021/nl102045g | *Nano Lett.* **XXXX,** *xxx,* 000–000

(27) Zhao, H.; Mazumdar, S. *Phys. Rev. Lett.* **2004**, *93*, 157402.
(28) Wang, F.; Cho, D. J.; Kessler, B.; Deslippe, J.; Schuck, P. J.; Louie, S. G.; Zettl, A.; Heinz, T. F.; Shen, Y. R. *Phys. Rev. Lett.* **2007**, *99*, 227401.
(29) Zeng, H.; Zhao, H.; Zhang, F.-C.; Cui, X. *Phys. Rev. Lett.* **2009**, *102*, 136406.
(30) Lakowicz, J. R. *Principles of Fluorescence Spectroscopy*; Kluwer Academic/Plenum Publishers: New York, 1999.
(31) Nirmal, M.; Dabbousi, B. O.; Bawendi, M. G.; Macklin, J. J.; Trautman, J. K.; Harris, T. D.; E., B. L. *Nature* **1996**, *383*, 802–804.
(32) van Sark, W.; Frederix, P.; Van den Heuvel, D.; Gerritsen, H.; Bol, A.; van Lingen, J.; Donega, C.; Meijerink, A. *J. Phys. Chem. B* **2001**, *105*, 8281–8284.
(33) Kukura, P.; Celebrano, M.; Renn, A.; Sandoghdar, V. *Nano Lett.* **2009**, *9*, 926–929.



DOI: 10.1021/nl102045g | *Nano Lett.* **XXXX,** *xxx,* 000–000